ATLAS CONF Note

ATLAS-CONF-2023-015

23rd March 2023

A precise determination of the strong-coupling constant from the recoil of Z bosons with the ATLAS experiment at $\sqrt{s} = 8$ TeV

The ATLAS Collaboration

The coupling constant of the strong force is determined from the transverse-momentum distribution of Z bosons produced in proton-proton collision at the LHC and recorded by the ATLAS experiment. The Z-boson cross sections are measured in the full phase space of the decay leptons using 15 million electron and muon pairs, in dataset corresponding to an integrated luminosity of 20.2 fb^{-1}. The analysis is based on predictions evaluated at third order in perturbative QCD, supplemented by the resummation of logarithmically-enhanced contributions in the small transverse-momentum region of the lepton pairs. The determined value of the strong coupling at the reference scale corresponding to the Z-boson mass is $\alpha_s(m_Z) = 0.11828^{+0.00084}_{-0.00088}$. This is the most precise experimental determination of $\alpha_s(m_Z)$ achieved so far.

1 Introduction

The coupling constant of the strong interaction is one of the fundamental parameters of the Standard Model, and is the least precisely known among the fundamental couplings in nature. The strong interaction is theoretically described by Quantum Chromodynamics (QCD), a gauge field theory with symmetry group SU(3) [1, 2]. The free parameters of QCD include the running coupling constant, $\alpha_s(Q^2)$, that runs with the energy scale Q^2 characterising the interaction, and six quark masses. While the running of the coupling constant is fully predicted by theory, its value at a reference scale needs to be determined experimentally. The most recent world average of experimental determinations and theoretical predictions from lattice QCD of the strong-coupling constant at the scale of the Z-boson mass yields $\alpha_s(m_Z) = 0.1179 \pm 0.0009$, with a relative uncertainty of 0.8% [3]. This uncertainty is orders of magnitude larger than that of the couplings of the other three fundamental interactions: the electromagnetic, weak, and gravitational forces.

Our knowledge of the strong-coupling constant has improved throughout the years, from the significant uncertainties of the first determinations in the mid 1980s [4], to the present uncertainty which is at the percent level. Further improving the precision of α_s is important to reduce the associated theoretical uncertainty which enters into all cross-section calculations for processes at the LHC, and affects several key observables at e^+e^- colliders. As an example, in the global fit of the electroweak sector of the Standard Model, the value of $\alpha_s(m_Z)$ is the leading source of uncertainty in the computation of the total and partial hadronic Z boson widths [5–7]. A precise determination of $\alpha_s(m_Z)$ is required to fully exploit the sensitivity to new physics of high-precision measurements of such observables at future colliders. The value of $\alpha_s(m_Z)$ and its energy evolution have also far-reaching implications including the stability of the electroweak vacuum [8], and the convergence of the couplings of the strong, weak and electromagnetic forces at an energy close to the Plank scale, which might signal the onset of a possible grand unification.

Various different determinations of $\alpha_s(m_Z)$ contribute to the current world average, and are categorised according to their methodological approach [9]. The most precise determinations are based on lattice QCD analysis of hadron spectroscopy, with a result of $\alpha_s(m_Z) = 0.1184 \pm 0.0008$ [10], and hadronic τ-lepton decays, with a result of $\alpha_s(m_Z) = 0.1177 \pm 0.0019$ [3, 11–16]. Only a few determinations are performed at next-to-next-to-next-to-leading order (N^3LO) in QCD, namely those from τ decays [11], and the global fit of the electroweak observables [6], yielding $\alpha_s(m_Z) = 0.1194 \pm 0.0029$. At hadron colliders, the strong-coupling constant has been determined in final states with jets [17, 18] from inclusive top quark pair production [19, 20], and more recently from inclusive W- and Z-boson production [21]. The high-momentum region of the Z-boson transverse-momentum (p_T) distribution measured at the LHC [22–24] was recently included in the determination of parton distribution functions (PDFs) [25], and contributed to the simultaneous determination of PDFs and the strong-coupling constant in Ref. [26]. Some of these determinations, in particular those with jets in the final state, allow probing the strong coupling at high values of momentum transfer. However, current hadron collider determinations generally suffer from large theoretical uncertainties, and do not provide a competitive determination of the strong-coupling constant at the scale of the Z-boson mass, $\alpha_s(m_Z)$.

Further improving the knowledge of $\alpha_s(m_Z)$ is limited by two important sources of theoretical uncertainty: the accuracy of the perturbative predictions and the size of non-perturbative effects. In this context, it is highly desirable to explore alternative determinations of $\alpha_s(m_Z)$, based on the most sensitive observables and state-of-the-art theory predictions. This paper presents a precise determination of $\alpha_s(m_Z)$ from a semi-inclusive (i.e. radiation inhibited) observable [27], namely the low-momentum Sudakov region[1] of

[1] The low-energy region of the transverse-momentum distribution of Z bosons is characterised by very high probability of gluon

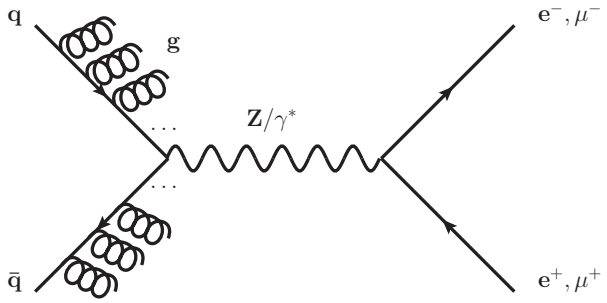

Figure 1: Leading-order Feynman diagram for the production of a massive electron or muon pair through the Drell-Yan process, including soft gluon radiation from the initial-state quarks.

the transverse-momentum distribution of Z bosons produced via the Drell-Yan process [29], which denotes the production of a massive lepton-pair in hadron-hadron collisions at high energies. The strong force is responsible for the radiation from the initial-state partons, and for the subsequent recoil of the Z bosons which acquire non-zero transverse momentum. The hardness of the transverse-momentum distribution is a measure of the strength of the recoil of the Z bosons, which in turn is proportional to the strong coupling. In this analysis, the QCD initial state radiative processes are used to determine the strong coupling, in contrast to most other determinations of $\alpha_s(m_Z)$ at hadron colliders which analyse observables using final state objects, and the energy scale at which the strong coupling is probed is unambigously fixed by the Z-boson mass. This methodology was tested in Ref. [30] using proton-antiproton collisions data at the Tevatron, and is here applied for the first time at the LHC.

Figure 1 depicts the leading-order Feynman diagram of the Drell-Yan process, with a schematic representation of soft gluon radiation from the initial-state quarks. Figure 2 shows the Z-boson transverse-momentum distribution for three different values of $\alpha_s(m_Z)$.

Compared to other determinations of $\alpha_s(m_Z)$ at hadron colliders based on either exclusive or inclusive observables, this determination gathers all desirable features for high precision: large observable sensitivity to $\alpha_s(m_Z)$ compared to the experimental precision, and high perturbative accuracy of the theoretical predictions [33–37], enabled by the computation of some perturbative corrections in QCD at four and five loops [38–42].

2 ATLAS detector

The ATLAS experiment [43] at the LHC is a multipurpose particle detector with a forward–backward symmetric cylindrical geometry and a near 4π coverage in solid angle.[2] It consists of an inner tracking detector surrounded by a thin superconducting solenoid providing a 2 T axial magnetic field, electromagnetic and hadron calorimeters, and a muon spectrometer. The inner tracking detector covers the pseudorapidity

emissions with vanishing small momenta. Rather than calculate each of these, it is theoretically simpler to model them as a single factor quantifying the probability of no emission, known as the Sudakov form factor [28].

[2] ATLAS uses a right-handed coordinate system with its origin at the nominal interaction point (IP) in the centre of the detector and the z-axis along the beam pipe. The x-axis points from the IP to the centre of the LHC ring, and the y-axis points upwards. Cylindrical coordinates (r, ϕ) are used in the transverse plane, ϕ being the azimuthal angle around the z-axis. The pseudorapidity is defined in terms of the polar angle θ as $\eta = -\ln\tan(\theta/2)$. Angular distance is measured in units of $\Delta R \equiv \sqrt{(\Delta\eta)^2 + (\Delta\phi)^2}$.

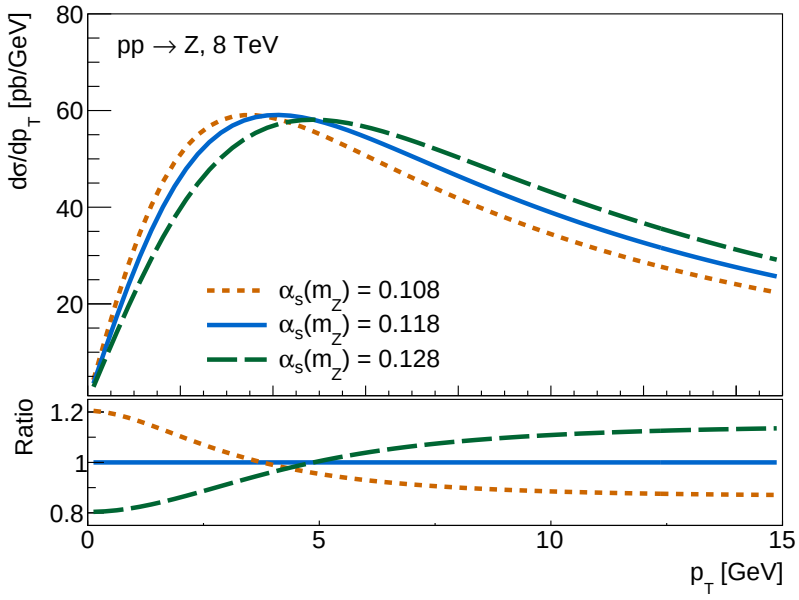

Figure 2: Transverse-momentum distribution of Z bosons predicted with `DYTurbo` [31] at different values of $\alpha_s(m_Z)$, using the MSHT20 PDF set [32].

range $|\eta| < 2.5$. It consists of silicon pixel, silicon microstrip, and transition radiation tracking detectors. Lead/liquid-argon (LAr) sampling calorimeters provide electromagnetic (EM) energy measurements with high granularity. A steel/scintillator-tile hadron calorimeter covers the central pseudorapidity range ($|\eta| < 1.7$). The endcap and forward regions are instrumented with LAr calorimeters for both the EM and hadronic energy measurements up to $|\eta| = 4.9$. The muon spectrometer surrounds the calorimeters and is based on three large superconducting air-core toroidal magnets with eight coils each. The field integral of the toroids ranges between 2.0 and 6.0 T m across most of the detector. The muon spectrometer includes a system of precision tracking chambers and fast detectors for triggering. A three-level trigger system is used to select events. The first-level trigger is implemented in hardware and uses a subset of the detector information to accept events at a rate of at most 75 kHz. This is followed by two software-based trigger levels that together reduce the accepted event rate to 400 Hz on average depending on the data-taking conditions during 2012. An extensive software suite [44] is used in data simulation, in the reconstruction and analysis of real and simulated data, in detector operations, and in the trigger and data acquisition systems of the experiment. The data were collected by the ATLAS detector in 2012 at a centre-of-mass energy of $\sqrt{s} = 8$ TeV, and correspond to an integrated luminosity of 20.2 fb^{-1}. The mean number of additional pp interactions per bunch crossing (pile-up events) in the data set is approximately 20.

3 Cross-section measurement

The Z-boson transverse-momentum distribution is measured in the electron and muon decay channels, which provide a clear signature with low background rates and a high precision measurement of the momentum, as presented in Ref. [45]. The double-differential cross sections as functions of transverse momentum and rapidity (y) of the Z boson are measured in the pole region, defined as $80 < m_{\ell\ell} < 100$ GeV, where $m_{\ell\ell}$ is the invariant mass of the dilepton system. The combination of 6.2 million electron and

7.8 million muon pairs in the central region of $|\eta| < 2.4$ is complemented by 1.3 million electron pairs with one electron in the forward region of the detector of $2.5 < |\eta| < 4.9$ and one electron in the central region. Electron candidates in the central region are required to have either $p_{\mathrm{T}} > 20$ GeV when paired to another central electron candidate, or $p_{\mathrm{T}} > 25$ GeV when paired to a forward electron candidate. Muon candidates are required to have $p_{\mathrm{T}} > 20$ GeV. Electron candidates in the forward region are required to have $p_{\mathrm{T}} > 20$ GeV.

The cross-section measurement relies on the decomposition of the lepton angular $\cos\theta$ and ϕ distributions in the Collins-Soper frame [46] into nine spherical harmonic polynomials, multiplied by angular coefficients, A_i [47]. The cross sections are extracted from the data by fitting templates of the spherical harmonics polynomial to the reconstructed angular distributions in $(\cos\theta, \phi)$. The decomposition is based on a simple and model-independent ansatz: the spin-one nature of the intermediate boson and spin-half nature of the decay leptons, and on the assumption of angular momentum conservation and quantisation. The measured cross sections are extrapolated to the unmeasured region of phase space by analytic continuation of the harmonic polynomials. The double-differential cross sections are measured in eight rapidity bins in the range $|y| < 3.6$. The choice of bin boundaries in p_{T} is the result of an optimisation with respect to the limited resolution of the measurements at low p_{T}. The region of Z-boson transverse momentum $p_{\mathrm{T}} < 29$ GeV is considered for the determination of $\alpha_{\mathrm{s}}(m_Z)$, corresponding to nine bins of transverse momentum, and a total of 72 bins. The total uncertainties in the measurements are dominated by the statistical uncertainties in the data and to a lesser extent in the simulation samples. They are below 1% for $|y| < 2.0$, and below 10% for $2.0 < |y| < 3.6$ [45].

4 Theoretical framework and statistical analysis

The theoretical predictions are computed with the public numerical program `DYTurbo` [31], which implements the resummation of logarithmically-enhanced contributions in the small-p_{T} region of the lepton pairs at approximate next-to-next-to-next-to-next-to-leading-logarithmic ($\mathrm{N^4LLa}$) accuracy [48], combined with the hard-collinear contributions at $\mathrm{N^3LO}$ in powers of the QCD coupling [33], and matched to fixed order at $\mathrm{N^3LO}$. The resummation is carried out in impact-parameter space b, which is the Fourier-conjugate variable to p_{T} [49–51]. The resummed cross section is given by the convolution of the leading-order (LO) cross section, the hard-collinear contributions, expanded in powers of α_{s}, and the universal (process-independent) Sudakov form factor which contains all the terms that order-by-order in α_{s} are logarithmically divergent as $p_{\mathrm{T}} \to 0$. A unitarity constraint is imposed in the matching to fixed order of the p_{T}-resummed prediction so as to recover exactly the $\mathrm{N^3LO}$ finite-order result upon integration over p_{T} of the full-lepton phase space resummed cross section. The $O(\alpha_{\mathrm{s}}^3)$ coefficient of the Z +jet cross section predictions, required for the matching to fixed order, was computed with MCFM [37, 52], using a lower cutoff of $p_{\mathrm{T}} = 5$ GeV, and the corresponding matching corrections were extrapolated down to $p_{\mathrm{T}} = 0$ by interpolating them with their known quadratic dependence on p_{T}/m_Z [53]. The Sudakov form factor is singular in the region of transverse-momenta of the order of the scale of the QCD coupling Λ_{QCD}. This signals that a truly non-perturbative region is approached and perturbative results are not reliable. Non-perturbative QCD effects are included with a corresponding form factor [49, 54], which depends on a set of parameters which are either left free in the fit for the determination of $\alpha_{\mathrm{s}}(m_Z)$, or varied at the time of assessing non-perturbative uncertainties.

The PDF set used in the predictions is the approximate $\mathrm{N^3LO}$ MSHT20 PDF set [55], which is the only PDF set currently available at this order. The PDFs are interpolated with LHAPDF [56] at the factorisation

scale μ_F, and evolved backward using the N^{3}LO solution of the evolution equation. The number of active flavours is set to five in all the coefficients entering the calculation, and in the evolution of the PDFs. The charm and bottom PDFs are asymptotically switched off in the backward evolution when approaching their corresponding thresholds.

The predicted cross sections depend on three unphysical scales: the renormalization scale μ_R, the factorization scale μ_F, and the resummation scale Q, which parameterizes the arbitrariness in the resummation procedure. The central value of the scales is set to the quadratic sum of $m_{\ell\ell}$ and p_{T}.

The effect of initial-state radiation of photons on the transverse-momentum shape is estimated at leading logarithmic accuracy with Pythia8 [57] and the AZ tune of parton shower parameters [22], and applied as a bin-by-bin multiplicative correction factor. Initial-state radiation of photons at next-to-leading logarithmic accuracy [58] is used to validate the Pythia8 predictions. Higher-order effects to the cross section normalisation from QED initial-state radiation and from electroweak virtual corrections are considered at next-to-leading order. These are directly computed using the code from Ref. [59], and are in agreement with the results from other calculations benchmarked in the LHC EW working group. At the Z pole, the virtual effects decrease the predicted cross-sections by 0.8%, while the QED initial-state effects increase them by 0.4%. These corrections are found to be independent of rapidity. Higher-order electroweak corrections are expected to be very small at the Z-boson pole, and neglected[3].

The statistical analysis for the determination of $\alpha_{\mathrm{s}}(m_Z)$ is performed with the xFitter framework [60]. The value of $\alpha_{\mathrm{s}}(m_Z)$ is determined by minimising a χ^2 function which includes both the experimental uncertainties and the theoretical uncertainties arising from PDF variations:

$$\chi^2(\beta_{\mathrm{exp}}, \beta_{\mathrm{th}}) = \sum_{i=1}^{N_{\mathrm{data}}} \frac{\left(\sigma_i^{\mathrm{exp}} + \sum_j \Gamma_{ij}^{\mathrm{exp}} \beta_{j,\mathrm{exp}} - \sigma_i^{\mathrm{th}} - \sum_k \Gamma_{ik}^{\mathrm{th}} \beta_{k,\mathrm{th}}\right)^2}{\Delta_i^2} + \sum_j \beta_{j,\mathrm{exp}}^2 + \sum_k \beta_{k,\mathrm{th}}^2 \,. \quad (1)$$

The correlated experimental and theoretical uncertainties are included using the nuisance parameter vectors β_{exp} and β_{th}, respectively. Their influence on the data and theory predictions is described by the $\Gamma_{ij}^{\mathrm{exp}}$ and $\Gamma_{ik}^{\mathrm{th}}$ matrices. The index i runs over all N_{data} data points, whereas the indices j and k correspond to the experimental and theoretical uncertainty nuisance parameters respectively. The measurements and the uncorrelated experimental uncertainties are given by σ_i^{exp} and Δ_i , respectively, and the theory predictions are σ_i^{th}. The matrices $\Gamma_{ij}^{\mathrm{exp}}$ encode all the information of the experimental covariance matrix of the measured double-differential cross sections as functions of transverse momentum and rapidity of the Z boson. The matrices $\Gamma_{ik}^{\mathrm{th}}$ cover the nuisance parameters of the PDF Hessian uncertainties, and parameters of the non-perturbative form factor, which are left free in the fit by adding unconstrained variations. The dependence of PDFs on the value of $\alpha_{\mathrm{s}}(m_Z)$ is accounted for by using corresponding α_{s}-series of PDF sets, which are provided for seven fixed values of $\alpha_{\mathrm{s}}(m_Z)$ in the range $0.114 < \alpha_{\mathrm{s}}(m_Z) < 0.120$. At each value of $\alpha_{\mathrm{s}}(m_Z)$, the PDF uncertainties are Hessian profiled and the χ^2 function is minimised by solving a system of linear equations, according to Eq. (1) [61], whereas the different values of χ^2 as a function of $\alpha_{\mathrm{s}}(m_Z)$ are minimised through a polynomial interpolation to determine $\alpha_{\mathrm{s}}(m_Z)$.

[3] The electroweak parameters are set according to the G_μ scheme, in which the Fermi coupling constant G_{F}, the W-boson mass m_W, and the Z-boson mass m_Z are set to the input values $G_{\mathrm{F}} = 1.1663787 \cdot 10^{-5}$ GeV^{-2}, $m_W = 80.385$ GeV, $m_Z = 91.1876$ GeV [16], whereas the weak-mixing angle and the QED coupling are calculated at tree level.

5 Determination of $\alpha_s(m_Z)$

A validation of the statistical analysis as well as an estimate of the sensitivity of the measured Z-boson cross-sections to $\alpha_s(m_Z)$ is quantified by a pseudofit. Identical theory predictions are used as central value for both data and theory in Eq. (1), including all statistical and systematic experimental uncertainties, and without theoretical uncertainties. The input value is set to $\alpha_s(m_Z) = 0.118$, and the pseudofit yields $\alpha_s(m_Z) = 0.11801 \pm 0.00006$. The closure of the method is thus found to be accurate to 0.01% and the relative uncertainty on $\alpha_s(m_Z)$ is estimated to be 0.05% before including the theoretical uncertainties discussed in the following.

The determination of $\alpha_s(m_Z)$ with the nominal settings and including experimental and PDF uncertainties in Eq. (1) yields $\alpha_s(m_Z) = 0.11847 \pm 0.00067$. The contribution to the uncertainty from the experimental sources and from the PDFs is estimated as ± 0.00044 and ± 0.00051 respectively. Uncertainties arising from missing higher orders in the truncation of the perturbative series are estimated through independent variations of μ_R, μ_F and Q in the range $m_{\ell\ell}/2 \leq \{\mu_R, \mu_F, Q\} \leq 2m_{\ell\ell}$ with the constraints $0.5 \leq \{\mu_F/\mu_R, Q/\mu_R, Q/\mu_F\} \leq 2$, leading to 14 variations.

The determined values of $\alpha_s(m_Z)$ range from a minimum of 0.11786 to a maximum of 0.11870. The midpoint of the scale variation envelope of $\alpha_s(m_Z) = 0.11828$ is taken as nominal result, and the scale variations envelope of ± 0.00042 is considered as an estimate of missing higher-order uncertainties.

The procedure is repeated at lower orders, starting from next-to-leading logarithmic accuracy matched to next-to-leading order (NLL+NLO). The MSHT20 PDF set is used throughout, and the order of the PDFs is matched to the order required by the logarithmic accuracy of the p_T-resummation, that is NNLO at N^{3}LL and NLO at NNLL[4]. The results are shown in Fig. 3. At every order, the estimate of missing higher order uncertainties obtained from the scale variations overlap with determinations of $\alpha_s(m_Z)$ at higher orders, giving confidence in the robustness and gradual convergence of these estimates.

Fits without the $O(\alpha_s^3)$ matching corrections yield a central value which is 0.00024 lower, and an increase in the half envelope of scale variations from ± 0.00042 to ± 0.00062, which is consistent with the observed shift. Uncertainties in the matching to the fixed order are estimated with fits in which the unitarity constraint is not applied. The scale variations midpoint and half envelope for these fits yield $\alpha_s(m_Z) = 0.11820 \pm 0.00037$. The difference between this set of fits and the nominal set of fits is taken as a matching uncertainty of -0.00008.

Uncertainties in the modelling of the non-perturbative form factor are estimated with variations of corresponding parameters, leading to an estimate of $^{+0.00012}_{-0.00020}$. The effect of charm and bottom quark masses and thresholds are estimated with various alternative fits, including variable-flavour number either in the evolution of the PDFs or in the running of α_s [62] in the Sudakov form factor, by varying the charm threshold μ_c by a factor of 2, and by varying the bottom thresholds μ_b by a factor of 0.5. The largest excursions are observed for the variable-flavour number PDF evolution, -0.00029, and for the variable-flavour number running of α_s, $+0.00021$, which are taken as an estimate of the uncertainty associated to the flavour model.

The inclusion of initial-state radiation of photons at leading logarithmic accuracy yields a shift on $\alpha_s(m_Z)$ of -0.00028. Half the value of such correction is considered as an uncertainty for missing higher order corrections for the initial-state radiation of photons. Initial-state radiation of photons at next-to-leading logarithmic accuracy [58] shifts the value of $\alpha_s(m_Z)$ by $+0.00007$, which is well within the

[4] At NLL the NLO PDF set is used, because the LO PDF set does not have $\alpha_s(m_Z)$ variations

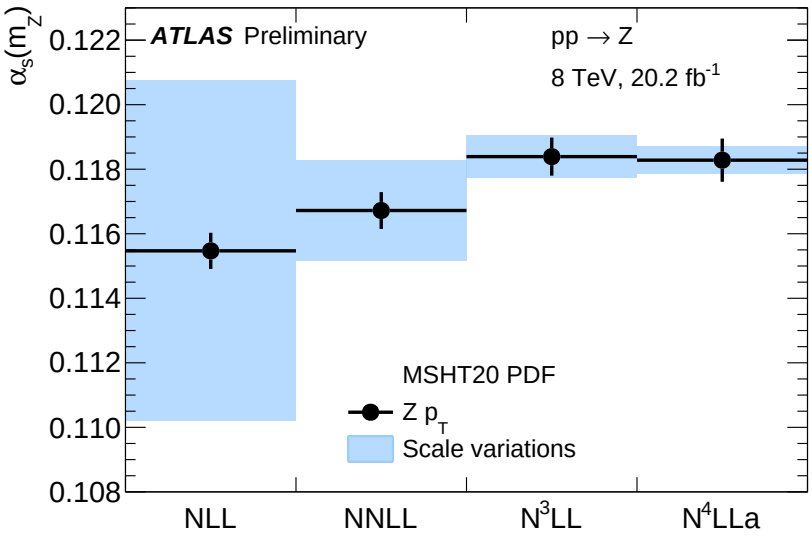

Figure 3: Determination of $\alpha_s(m_Z)$ at various different orders in the QCD perturbative expansion, using the MSHT20 PDF set. The filled area represents missing higher order uncertainties estimated through scale variations, the vertical error bars include experimental and PDF uncertainties.

Table 1: Summary of the uncertainties for the determination of $\alpha_s(m_Z)$.

Experimental uncertainty	+0.00044	-0.00044
PDF uncertainty	+0.00051	-0.00051
Scale variations uncertainties	+0.00042	-0.00042
Matching to fixed order	0	-0.00008
Non-perturbative model	+0.00012	-0.00020
Flavour model	+0.00021	-0.00029
QED ISR	+0.00014	-0.00014
N4LL approximation	+0.00004	-0.00004
Total	+0.00084	-0.00088

quoted uncertainty. The inclusion of NLO electroweak corrections yields a shift on $\alpha_s(m_Z)$ of +0.00006, uncertainties related to missing electroweak higher orders are considered negligible.

Uncertainties related to the numerical approximation or the incomplete knowledge of some of the coefficients required for N^{4}LL accuracy of p_T-resummation are estimated to contribute at the level of ±0.00004, with the largest contribution coming from the numerical approximation of the *cusp* anomalous dimension at five loops [39], and from the incomplete knowledge of the hard-collinear contributions at four loops [42]. Uncertainties due to the numerical approximation of the four loop splitting functions are already included in the MSHT20 PDF uncertainties.

A summary of the uncertainties in the determination of $\alpha_s(m_Z)$ is shown in Table 1.

The goodness of fit is assessed by computing the value of the χ^2 function with the theory predictions

evaluated at the measured value of $\alpha_s(m_Z)$ and at the best values of the non-perturbative parameters and of the QCD scales. In addition to the PDF uncertainties included in Eq. (1), all theory uncertainties considered in the analysis are added as theory nuisance parameters. The estimated χ^2 is 82 per 72 data points, corresponding to a p-value of 0.2.

Variations of the upper end of the fit range, are performed to test the stability of the results with respect to missing higher order corrections in the matching to fixed order. When lowering the upper end from 29 to 22 GeV a shift of $\alpha_s(m_Z)$ of -0.00017 and an increase of the estimate of missing higher order uncertainties from 0.00042 to 0.00050 is observed. When raising the upper end to 40.4 GeV a shift of $\alpha_s(m_Z)$ of $+0.00028$ and an increase of the estimate of missing higher order uncertainties to 0.00088 is observed. The shifts in the central values are compatible with the increase in missing higher order uncertainties.

The fit range is also varied by excluding the low transverse-momentum region. The range is reduced up to $5 < p_T < 29$ GeV, with a spread in the values of $\alpha_s(m_Z)$ at the level of $^{+0.00017}_{-0.00010}$, compatible with the increase in the uncertainty of the fit, from 0.00067 to 0.00071. Since the low transverse-momentum region of $p_T < 5$ GeV is the most sensitive to the non-perturbative and quark-flavour effects, this test provides a strong validation of the modelling of these corrections.

The post-fit predictions are compared to the measured Z-boson transverse-momentum distribution in Fig. 4. The overall shift of the normalisation is accounted for by a pull of the 1.8% luminosity uncertainty of 1.3 standard deviations.

The determination of $\alpha_s(m_Z)$ is repeated at a lower order, N^{3}LL+N^{3}LO, with the MSHT20, CT18A, NNPDF40 and HERAPDF20 NNLO PDF sets. The spread of the fitted values of $\alpha_s(m_Z)$ is ± 0.00102, driven by the difference between CT18A and NNPDF40. While these PDF sets are not appropriate for the present measurement given their reduced theoretical accuracy, this study provides a conservative estimate of the residual PDF model dependence of the result, demonstrating the excellent accuracy achievable compared to other methods of extracting $\alpha_s(m_Z)$. At this order, in addition to the Hessian profiling approach, a simultaneous determination of $\alpha_s(m_Z)$, PDFs and non-perturbative parameters is performed through the numerical minimisation of the χ^2 in the full-dimensional parameters space. The combined NC and CC DIS cross-section data from the H1 and ZEUS experiments at the HERA collider [63] are included in the fit, with a minimum four-momentum transfers Q^2 of 10 GeV^2, together with the measured Z-boson transverse-momentum cross sections. The determined value of $\alpha_s(m_Z)$ from this fit is 0.11777 ± 0.00065, where the quoted uncertainty is the uncertainty from the fit, which includes experimental and PDF uncertainties. The determined value of $\alpha_s(m_Z)$ is in agreement with corresponding determinations with the Hessian profiling approach at this order, and the uncertainty is comparable with the uncertainty of the nominal fit. At N^{3}LL+N^{3}LO, missing higher order uncertainties estimated with scale variations amount to ± 0.00066. Considering all the other relevant uncertainties listed in Table 1, the result of this determination is $\alpha_s(m_Z) = 0.11777^{+0.00097}_{-0.00100}$.

6 Outlook

The coupling constant of the strong force is determined from the measurement of the transverse-momentum distribution of Z bosons at a centre-of-mass energy of $\sqrt{s} = 8$ TeV. The analysis is based on a semi-inclusive observable at hadron-hadron colliders, and employs QCD resummed theory predictions. Contrary to other hadron collider observables, the Z-boson transverse-momentum distribution in the Sudakov region is not included in PDF fits, therefore largely reducing the issue of correlation of this $\alpha_s(m_Z)$

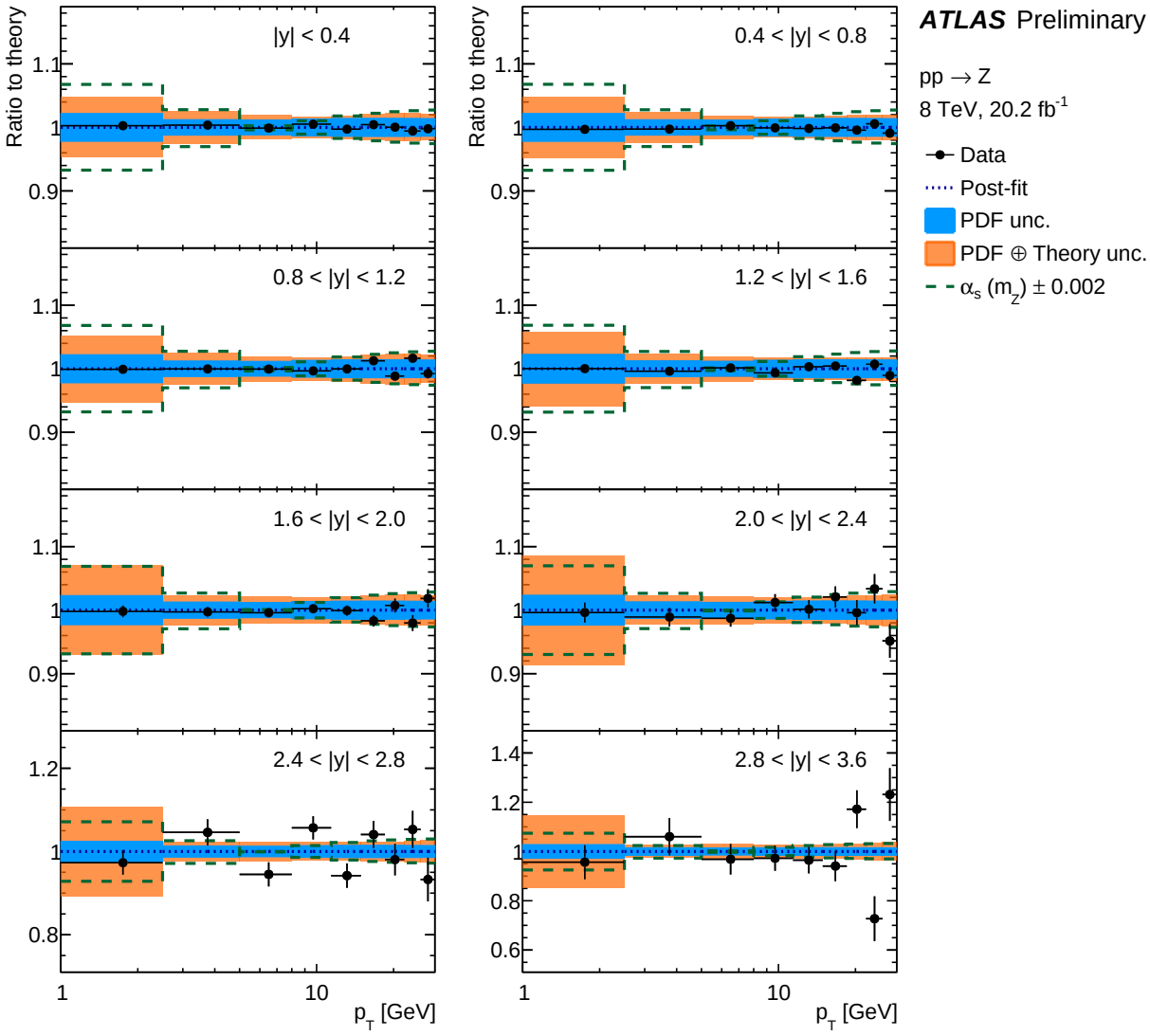

Figure 4: Ratios of double-differential measured cross sections as functions of transverse-momentum and rapidity of the Z boson to post-fit predictions. The blue band shows the PDF uncertainties of the predictions pulled and constrained by the fit, the orange band show the quadratic sum of PDF and all other theoretical uncertainties. The measured cross sections are corrected by the post-fit pull of the luminosity uncertainty, the vertical error bars show the experimental uncertainties of the measurement. The dashed lines show post-fit predictions in which $\alpha_s(m_Z)$ is varied by ±0.002 and all other parameters are kept fixed.

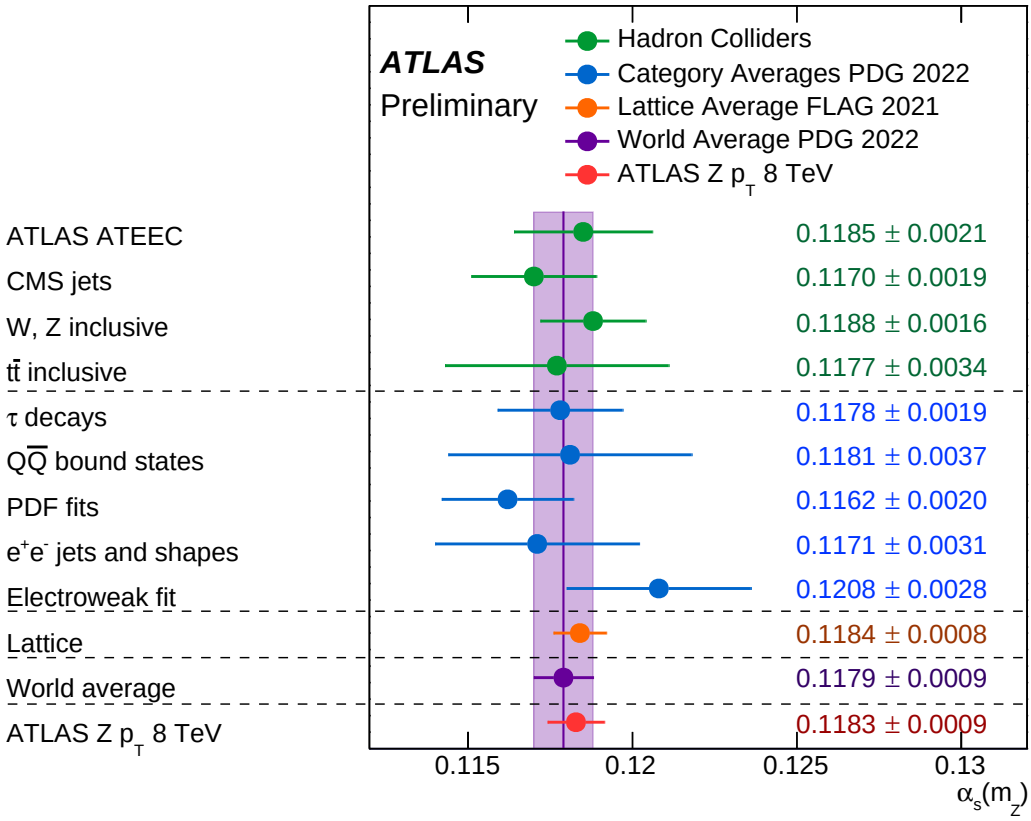

Figure 5: Comparison of the determination of $\alpha_s(m_Z)$ from the Z-boson transverse-momentum distribution with other determinations at hadron colliders [17, 18, 20, 21], with the PDG category averages [3], with the lattice QCD determination [10], and with the PDG world average.

determination with simultaneous determination of PDFs and strong-coupling constant. The measured value of $\alpha_s(m_Z) = 0.11828^{+0.00084}_{-0.00088}$ is compatible with other determinations and with the world-average value, as illustrated in Fig. 5.

Among experimental determinations, this is the most precise to date and the first based on N^{4}LLa+N^{3}LO predictions in perturbative QCD. This result marks the start of a new era in precision studies of QCD with the Drell-Yan process. The strong-coupling constant can be investigated with higher precision and in higher energy regimes with future larger datasets.

A Modelling of non-perturbative effects

Determinations of $\alpha_s(m_Z)$ are affected by non-perturbative power corrections of the type $\Lambda^p_{\rm QCD}/Q^p$, where $\Lambda_{\rm QCD}$ is the non-perturbative scale of QCD and Q is the order of magnitude of the momentum transfer in the process. Their impact strongly depends on the value of the power p for the given process used to determine $\alpha_s(m_Z)$. Non-perturbative QCD effects [49, 54, 64–72], are expected to be quadratically suppressed for the Drell-Yan $p_{\rm T}$ distribution [73], thanks to the azimuthal symmetry of the intrinsic transverse momentum smearing of partons [74, 75].

In the case of the Z-boson $p_{\rm T}$-resummed predictions used in this analysis, the Sudakov form factor is singular in the region of transverse-momenta of the order of the scale of the QCD coupling $\Lambda_{\rm QCD}$. This signals that a truly non-perturbative region is approached and perturbative results are not reliable. The singular behaviour of the perturbative form factor is removed by using the so-called b_* [49, 76] regularisation procedure, in which the dependence of the Sudakov form factor on the impact parameter b is frozen before reaching the singular point by performing the replacement $b^2 \to b_*^2 = b^2 b_{\rm lim}^2/(b^2 + b_{\rm lim}^2)$. In the calculation the default value of $b_{\rm lim} = 2$ GeV^{-1} is used. They are included in this analysis with a non-perturbative form factor [49, 54]:

$$S_{\rm NP}(b) = \exp\left[-g_j(b) - g_K(b)\log\frac{m_{\ell\ell}^2}{Q_0^2}\right] \tag{2}$$

with

$$g_j(b) = \frac{g\,b^2}{\sqrt{1+\lambda\,b^2}} + \text{sign}(q)\left(1 - \exp\left[-|q|\,b^4\right]\right) \tag{3}$$

$$g_K(b) = g_0\left(1 - \exp\left[-\frac{C_F\alpha_s(b_0/b_*)b^2}{\pi g_0\, b_{\rm lim}^2}\right]\right), \tag{4}$$

where $b_0 = 2e^{-\gamma_E}$, and γ_E is the Euler number. The g and q parameters represent the leading quadratic and quartic terms which are dominant in the region of moderate $p_{\rm T}$ of 4–10 GeV, where the sensitivity to $\alpha_s(m_Z)$ is maximal, and they are left free in the fit. The parameter λ controls the scale of transition from quadratic (Gaussian) to linear (exponential) behaviour of the non-perturbative primordial $k_{\rm T}$, which is expected to be of order of 0.3 fm [77]. It is set to 1 GeV^2 and varied at the time of assessing uncertainties of the non-perturbative model. The parameter g_0 controls the asymptotic behaviour of the non-perturbative form factor at very small $p_{\rm T}$, in a region where the measured cross section and the determined value of $\alpha_s(m_Z)$ have very little sensitivity. It is set to 0.3 GeV^2 [54] and varied at the time of assessing uncertainties of the non-perturbative model. The parameters $b_{\rm lim}$ and Q_0 represent respectively the scale at which the running of α_s is frozen, and the starting scale at which the non-perturbative form factor is parameterised by the function $g_j(b)$. Changes in these parameters should be completely reabsorbed by changes in the functions $g_K(b)$ and $g_j(b)$, provided they are flexible enough. Variations of $b_{\rm lim}$ and of Q_0 are performed to assess the uncertainty related to the choice of parameterization in Eqs. (2–4).

The value of g determined in the nominal fit is $g = 0.54 \pm 0.04$ GeV^2, with a correlation to $\alpha_s(m_Z)$ of -0.6, the value of q determined in the fit is $q = -0.06 \pm 0.04$ GeV^4, with a correlation to $\alpha_s(m_Z)$ of $+0.4$. The correlation between g and q is -0.7. Uncertainties in the modelling of the non-perturbative form factor are estimated with variations of the parameters $b_{\rm lim}$, Q_0, g_0, and λ. Variations of $b_{\rm lim}$ in the range 1.5 to 2.5 GeV^{-1} yield variations of $\alpha_s(m_Z)$ of $^{+0.00012}_{-0.00020}$. Variations of Q_0 in the range 0.5 to 2 GeV yield

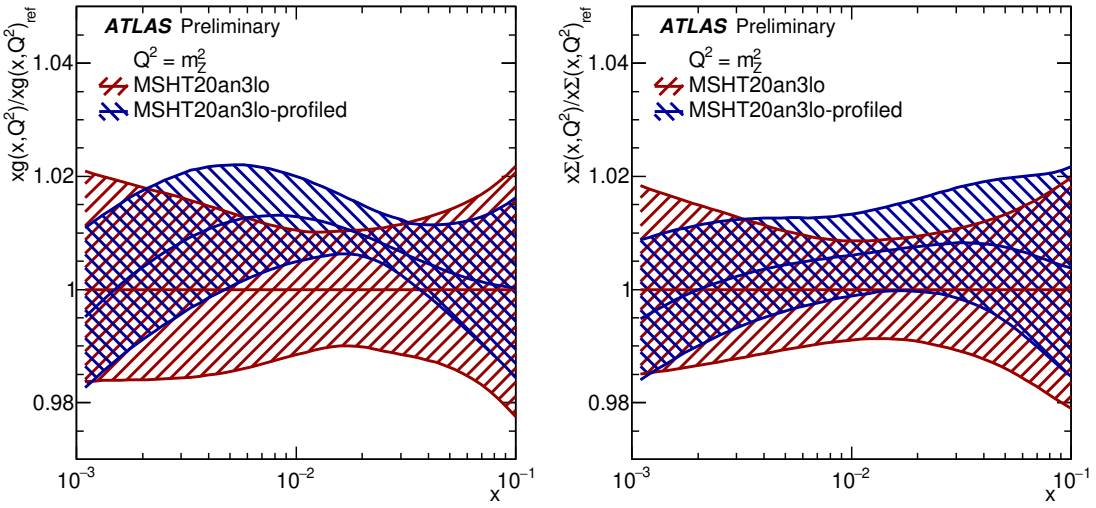

Figure 6: Ratios of the profiled gluon (left) and sea quark (right) PDFs to their initial values, at the scale $q^2 = m_Z^2$. The error bands represent the 68% confidence level.

variations on $\alpha_s(m_Z)$ of $^{+0.00006}_{-0.00002}$. Variations of g_0 in the range 0.1 to 0.5 GeV^2 yield variations on $\alpha_s(m_Z)$ which at the level of ± 0.00002. Variations of λ in the range from 0.5 GeV^2 to 2 GeV^2 yield variations on $\alpha_s(m_Z)$ of $^{+0.00011}_{-0.00019}$ The envelope of these variations is $^{+0.00012}_{-0.00020}$, which is considered as an estimate of the uncertainty of the non-perturbative model.

B PDF profiling

Pulls and constraints of the nuisance parameters associated to the PDF uncertainties in Eq. (1) can be reinterpreted in the PDF space through a Hessian profiling procedure [61]. Such a reinterpretation provide valuable information on the sensitivity of the measured cross sections to the PDFs. The largest effects are observed on the gluon and sea quarks PDFs, which are shown in Figure 6.

C Fits with NNLO PDFs

At order N^{4}LLa+N^{3}LO only one N^{3}LO PDF set is currently available, namely the MSHT20an3lo [55] PDF set. In order to study the dependence of the results on the choice of the PDF set, fits are performed at a lower order, N^{3}LL+N^{3}LO, using NNLO PDF sets. Table 2 shows results of fits with various different PDF sets. At this order, we observe a spread in the values of $\alpha_s(m_Z)$ extracted with different PDF sets of ± 0.00102, which is driven by the difference between the NNPDF4.0 and CT18A PDF sets.

The determination of $\alpha_s(m_Z)$ from the transverse-momentum distribution of Z-boson, is particularly sensitive to the gluon PDF. The PDFs determinations at NNLO are affected by significant tension between the low- and high-x gluon PDF, which is ascribed to tensions between datasets sensitive to the gluon PDFs, as inclusive deep-inelastic scattering at the HERA collider, hadron collider jets measurements, top pair production, and Z-boson p_T measurements in the high transverse-momentum region.

Table 2: Summary of N^{3}LL fits with NNLO PDFs.

PDF set	$\alpha_s(m_Z)$	PDF uncertainty	g [GeV^2]	q [GeV^4]	χ^2/dof
MSHT20 [32]	0.11839	0.00040	0.44	-0.07	96.0 /69
NNPDF40 [78]	0.11779	0.00024	0.50	-0.08	116.0/69
CT18A [79]	0.11982	0.00050	0.36	-0.03	97.7 /69
HERAPDF20 [63]	0.11890	0.00027	0.40	-0.04	132.3/69

In order to investigate the effect of these tensions on the determination of $\alpha_s(m_Z)$ at N^{3}LL, fits are performed in which also the combined NC and CC DIS cross-section data from the H1 and ZEUS experiments at the HERA collider [63] are included, with a minimum Q^2 value of 10 GeV^2, together with the measured Z-boson transverse-momentum cross sections. The HERA data are already included in all PDF fits, they are re-included here to the purpose of lessening the impact of other datasets on the gluon PDF. After the inclusion of HERA data in the fit the half-envelope of the PDF sets considered is reduced to ±0.00016.

The approximate N^{3}LO PDF fit of MSHT20, which is used as the nominal result, largely reduces the tension in the gluon PDF, as indicated by the significant improvement in the χ^2 associated to the Z-boson p_T measurement in the high transverse-momentum region [55]. These observations support that the spread of $\alpha_s(m_Z)$ using different PDF sets at NNLO is not representative of the true PDF uncertainty at N^{3}LO. However, further studies are needed to verify the robustness of the estimate of the PDF uncertainties at N^{3}LO in the MSHT20 analysis, when other PDF determinations at this order become available.

D Combined fits of $\alpha_s(m_Z)$ and PDFs

Determinations of $\alpha_s(m_Z)$ at hadron colliders are exposed to possible biases unless the PDFs are determined simultaneously along with $\alpha_s(m_Z)$ [80]. The Hessian profiling employed in this analysis provides an approximation to a PDF determination which relies on the accuracy of the quadratic approximation around the minimum [81]. In the nominal fit of $\alpha_s(m_Z)$ at N^{4}LLa+N^{3}LO, pulls and constraints of the nuisance parameters associated to the PDF uncertainties are below one sigma and 30%, respectively, indicating that the new minimum of the profiled PDFs is close to the original minimum, which gives confidence in the validity of the quadratic approximation.

A simultaneous determination of $\alpha_s(m_Z)$, PDFs and non-perturbative parameters through the numerical minimisation of the χ^2 in the full-dimensional parameters space [82] is performed at N^{3}LL+N^{3}LO, with PDFs evolved at NNLO. The combined NC and CC DIS cross-section data from the H1 and ZEUS experiments at the HERA collider [63] are included, with a minimum four-momentum transfers Q^2 of 10 GeV^2, together with the measured Z-boson transverse-momentum cross sections.

The light-quark coefficient functions of the DIS cross sections are calculated in the $\overline{MS}$ scheme [83], and with the renormalisation and factorisation scales set to the four momentum transfers Q^2. The heavy quarks c and b are dynamically generated, and the corresponding coefficient functions for the neutral-current processes with γ^* exchange are calculated in the general-mass variable-flavour-number scheme [84–86], with up to five active quark flavours. The charm mass is set to $m_c = 1.43$ GeV, and the bottom mass to $m_b = 4.50$ GeV [63]. For the charged-current processes the heavy quarks are treated as massless.

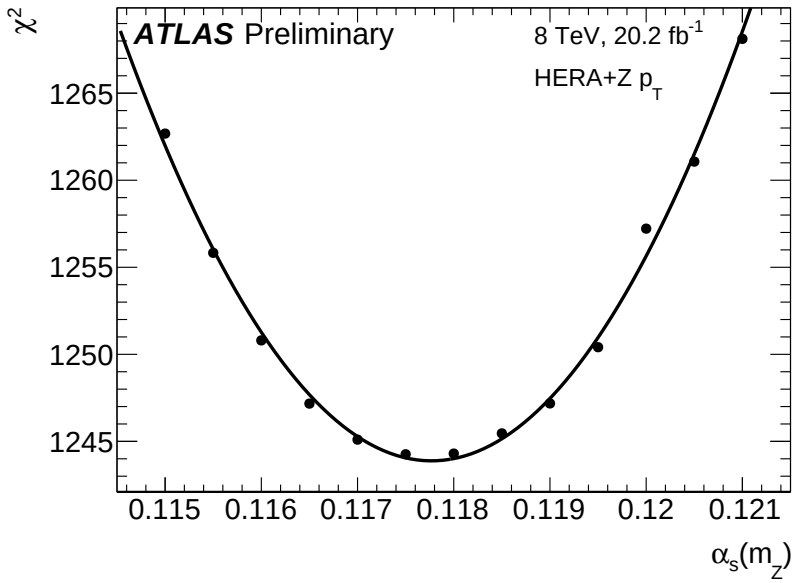

Figure 7: Values of the χ^2 function for the determination of $\alpha_s(m_Z)$ from a combined fit of PDFs and non-perturbative parameters.

The PDFs for the gluon, u-valence, d-valence, $\bar{u}$, $\bar{d}$ quark densities are parameterised at the input scale $Q_0^2 = 1.9$ GeV^2 with the parametrisation of Ref. [87]. The contribution of the s-quark density is taken to be proportional to the $\bar{d}$-quark density by setting $x\bar{s}(x) = r_s x\bar{d}(x)$, with $r_s = 0.67$.

Fits are performed at fixed values of $\alpha_s(m_Z)$, and the fitted value of $\alpha_s(m_Z)$ is determined from a quadratic interpolation of the χ^2 as a function of $\alpha_s(m_Z)$, as shown in Fig. 7. The determined value of $\alpha_s(m_Z)$ is 0.11777 ± 0.00065, where the quoted uncertainty is the uncertainty from the fit, which includes experimental and PDF uncertainties. The value of $\alpha_s(m_Z)$ is in agreement with corresponding determinations with the Hessian profiling approach at this order, as shown in Table 2, and the uncertainty is comparable with the uncertainty of the nominal fit of 0.00067.

E Sudakov subleading higher-order corrections

Additional fits are performed which differ with the nominal fit for subleading higher order corrections in the Sudakov form factor. In Ref. [88] different procedures for the computation of the Sudakov form factor are discussed, including analytic and numerical solutions. Subleading corrections in the definition of the Sudakov form factor and in the running of α_s are tested with fits where the Sudakov form factor is evaluated with a numerical integration, and $\alpha_s(Q^2)$ in the Sudakov form factor is obtained from the exact numerical renormalisation-group-equation invariant solution for the running of α_s. Scale variations are estimated with the methodology proposed in Ref. [89]. The scale variations midpoint and half envelope for these fits yield $\alpha_s(m_Z) = 0.11832 \pm 0.00029$. Fits where the hard-collinear coefficients are evolved according to the CSS scheme [49] yield a value of $\alpha_s(m_Z) = 0.11872$ for the central value of the scales. In all the cases considered, the inclusion of subleading higher order corrections is covered by the estimate of missing higher order corrections based on scale variations, hence no additional uncertainty is considered.

References

[1] D. J. Gross and F. Wilczek, *Ultraviolet Behavior of Non-Abelian Gauge Theories*, Phys. Rev. Lett. **30** (1973) 1343, ed. by J. C. Taylor (cit. on p. 2).

[2] H. D. Politzer, *Reliable Perturbative Results for Strong Interactions?*, Phys. Rev. Lett. **30** (1973) 1346, ed. by J. C. Taylor (cit. on p. 2).

[3] R. L. Workman et al., *Review of Particle Physics*, PTEP **2022** (2022) 083C01 (cit. on pp. 2, 11).

[4] M. Aguilar-Benitez et al., *Review of Particle Properties. Particle Data Group*, Phys. Lett. B **170** (1986) 1 (cit. on p. 2).

[5] S. Heinemeyer, S. Jadach and J. Reuter, *Theory requirements for SM Higgs and EW precision physics at the FCC-ee*, Eur. Phys. J. Plus **136** (2021) 911, arXiv: 2106.11802 [hep-ph] (cit. on p. 2).

[6] GFitter Group, J. Haller et al., *Update of the global electroweak fit and constraints on two-Higgs-doublet models*, Eur. Phys. J. C **78** (2018) 675, arXiv: 1803.01853 [hep-ph] (cit. on p. 2).

[7] D. d'Enterria and V. Jacobsen, *Improved strong coupling determinations from hadronic decays of electroweak bosons at N^3LO accuracy*, (2020), arXiv: 2005.04545 [hep-ph] (cit. on p. 2).

[8] G. Degrassi et al., *Higgs mass and vacuum stability in the Standard Model at NNLO*, JHEP **08** (2012) 098, arXiv: 1205.6497 [hep-ph] (cit. on p. 2).

[9] G. Salam, 'The strong coupling: a theoretical perspective', *From My Vast Repertoire ...: Guido Altarelli's Legacy*, ed. by A. Levy, S. Forte and G. Ridolfi, 2019, chap. 7 101, arXiv: 1712.05165 [hep-ph], URL: https://www.worldscientific.com/doi/abs/10.1142/9789813238053_0007 (cit. on p. 2).

[10] Y. Aoki et al., *FLAG Review 2021*, (2021), arXiv: 2111.09849 [hep-lat] (cit. on pp. 2, 11).

[11] P. A. Baikov, K. G. Chetyrkin and J. H. Kuhn, *Order α_s^4 QCD Corrections to Z and τ Decays*, Phys. Rev. Lett. **101** (2008) 012002, arXiv: 0801.1821 [hep-ph] (cit. on p. 2).

[12] A. Pich and A. Rodríguez-Sánchez, *Determination of the QCD coupling from ALEPH τ decay data*, Phys. Rev. D **94** (2016) 034027, arXiv: 1605.06830 [hep-ph] (cit. on p. 2).

[13] M. Davier, A. Höcker, B. Malaescu, C.-Z. Yuan and Z. Zhang, *Update of the ALEPH non-strange spectral functions from hadronic τ decays*, Eur. Phys. J. C **74** (2014) 2803, arXiv: 1312.1501 [hep-ex] (cit. on p. 2).

[14] D. Boito et al., *Strong coupling from $e^+e^- \to$ hadrons below charm*, Phys. Rev. D **98** (2018) 074030, arXiv: 1805.08176 [hep-ph] (cit. on p. 2).

[15] D. Boito et al., *Strong coupling from an improved τ vector isovector spectral function*, Phys. Rev. D **103** (2021) 034028, arXiv: 2012.10440 [hep-ph] (cit. on p. 2).

[16] P. A. Zyla et al., *Review of Particle Physics*, PTEP **2020** (2020) 083C01 (cit. on pp. 2, 6).

[17] CMS Collaboration, *Measurement and QCD analysis of double-differential inclusive jet cross sections in proton–proton collisions at $\sqrt{s} = 13$ TeV*, JHEP **02** (2021) 142, arXiv: 2111.10431 [hep-ex] (cit. on pp. 2, 11).

[18] ATLAS Collaboration, *Determination of the strong coupling constant from transverse energy–energy correlations in multijet events at $\sqrt{s} = 13$ TeV with the ATLAS detector*, (2023), arXiv: 2301.09351 [hep-ex] (cit. on pp. 2, 11).

[19] CMS Collaboration, *Measurement of the $t\bar{t}$ production cross section, the top quark mass, and the strong coupling constant using dilepton events in pp collisions at $\sqrt{s} = 13$ TeV*, Eur. Phys. J. C **79** (2019) 368, arXiv: 1812.10505 [hep-ex] (cit. on p. 2).

[20] T. Klijnsma, S. Bethke, G. Dissertori and G. P. Salam, *Determination of the strong coupling constant $\alpha_s(m_Z)$ from measurements of the total cross section for top-antitop quark production*, Eur. Phys. J. C **77** (2017) 778, arXiv: 1708.07495 [hep-ph] (cit. on pp. 2, 11).

[21] D. d'Enterria and A. Poldaru, *Extraction of the strong coupling $\alpha_s(m_Z)$ from a combined NNLO analysis of inclusive electroweak boson cross sections at hadron colliders*, JHEP **06** (2020) 016, arXiv: 1912.11733 [hep-ph] (cit. on pp. 2, 11).

[22] ATLAS Collaboration, *Measurement of the Z/γ^* boson transverse momentum distribution in pp collisions at $\sqrt{s} = 7$ TeV with the ATLAS detector*, JHEP **09** (2014) 145, arXiv: 1406.3660 [hep-ex] (cit. on pp. 2, 6).

[23] ATLAS Collaboration, *Measurement of the transverse momentum and ϕ^*_η distributions of Drell-Yan lepton pairs in proton–proton collisions at $\sqrt{s} = 8$ TeV with the ATLAS detector*, Eur. Phys. J. C **76** (2016) 291, arXiv: 1512.02192 [hep-ex] (cit. on p. 2).

[24] CMS Collaboration, *Measurement of the Z boson differential cross section in transverse momentum and rapidity in proton–proton collisions at 8 TeV*, Phys. Lett. B **749** (2015) 187, arXiv: 1504.03511 [hep-ex] (cit. on p. 2).

[25] R. Boughezal, A. Guffanti, F. Petriello and M. Ubiali, *The impact of the LHC Z-boson transverse momentum data on PDF determinations*, JHEP **07** (2017) 130, arXiv: 1705.00343 [hep-ph] (cit. on p. 2).

[26] R. D. Ball et al., *Precision determination of the strong coupling constant within a global PDF analysis*, Eur. Phys. J. C **78** (2018) 408, arXiv: 1802.03398 [hep-ph] (cit. on p. 2).

[27] S. Catani, B. R. Webber and G. Marchesini, *QCD coherent branching and semi-inclusive processes at large x*, Nucl. Phys. B **349** (1991) 635 (cit. on p. 2).

[28] V. V. Sudakov, *Vertex parts at very high-energies in quantum electrodynamics*, Sov. Phys. JETP **3** (1956) 65 (cit. on p. 3).

[29] S. D. Drell and T.-M. Yan, *Massive Lepton-Pair Production in Hadron-Hadron Collisions at High Energies*, Phys. Rev. Lett. **25** (1970) 316, [Erratum: Phys.Rev.Lett. 25, 902 (1970)] (cit. on p. 3).

[30] S. Camarda, G. Ferrera and M. Schott, *Determination of the strong-coupling constant from the Z-boson transverse-momentum distribution*, (2022), arXiv: 2203.05394 [hep-ph] (cit. on p. 3).

[31] S. Camarda et al., *DYTurbo: Fast predictions for Drell-Yan processes*, Eur. Phys. J. C **80** (2020) 251, [Erratum: Eur.Phys.J.C 80, 440 (2020)], arXiv: 1910.07049 [hep-ph] (cit. on pp. 4, 5).

[32] S. Bailey, T. Cridge, L. A. Harland-Lang, A. D. Martin and R. S. Thorne,
Parton distributions from LHC, HERA, Tevatron and fixed target data: MSHT20 PDFs,
Eur. Phys. J. C **81** (2021) 341, arXiv: 2012.04684 [hep-ph] (cit. on pp. 4, 14).

[33] S. Camarda, L. Cieri and G. Ferrera, *Drell–Yan lepton-pair production: q_T resummation at* $\mathrm{N^3LL}$ *accuracy and fiducial cross sections at* $\mathrm{N^3LO}$, Phys. Rev. D **104** (2021) L111503,
arXiv: 2103.04974 [hep-ph] (cit. on pp. 3, 5).

[34] E. Re, L. Rottoli and P. Torrielli,
Fiducial Higgs and Drell-Yan distributions at N^3LL'+NNLO with RadISH, JHEP **09** (2021) 108,
arXiv: 2104.07509 [hep-ph] (cit. on p. 3).

[35] W.-L. Ju and M. Schönherr,
The q_T and $\Delta\phi$ spectra in W and Z production at the LHC at N^3LL'+N^2LO, JHEP **10** (2021) 088,
arXiv: 2106.11260 [hep-ph] (cit. on p. 3).

[36] X. Chen et al., *Third-Order Fiducial Predictions for Drell-Yan Production at the LHC*,
Phys. Rev. Lett. **128** (2022) 252001, arXiv: 2203.01565 [hep-ph] (cit. on p. 3).

[37] T. Neumann and J. Campbell, *Fiducial Drell-Yan production at the LHC improved by transverse-momentum resummation at* $\mathrm{N^4LL_p + N^3LO}$, Phys. Rev. D **107** (2023) L011506,
arXiv: 2207.07056 [hep-ph] (cit. on pp. 3, 5).

[38] P. A. Baikov, K. G. Chetyrkin and J. H. Kühn, *Five-Loop Running of the QCD coupling constant*,
Phys. Rev. Lett. **118** (2017) 082002, arXiv: 1606.08659 [hep-ph] (cit. on p. 3).

[39] F. Herzog et al., *Five-loop contributions to low-N non-singlet anomalous dimensions in QCD*,
Phys. Lett. B **790** (2019) 436, arXiv: 1812.11818 [hep-ph] (cit. on pp. 3, 8).

[40] C. Duhr, B. Mistlberger and G. Vita,
Four-Loop Rapidity Anomalous Dimension and Event Shapes to Fourth Logarithmic Order,
Phys. Rev. Lett. **129** (2022) 162001, arXiv: 2205.02242 [hep-ph] (cit. on p. 3).

[41] I. Moult, H. X. Zhu and Y. J. Zhu, *The four loop QCD rapidity anomalous dimension*,
JHEP **08** (2022) 280, arXiv: 2205.02249 [hep-ph] (cit. on p. 3).

[42] A. Chakraborty et al.,
Hbb vertex at four loops and hard matching coefficients in SCET for various currents,
Phys. Rev. D **106** (2022) 074009, arXiv: 2204.02422 [hep-ph] (cit. on pp. 3, 8).

[43] ATLAS Collaboration, *The ATLAS Experiment at the CERN Large Hadron Collider*,
JINST **3** (2008) S08003 (cit. on p. 3).

[44] ATLAS Collaboration, *The ATLAS Collaboration Software and Firmware*,
ATL-SOFT-PUB-2021-001, 2021, URL: https://cds.cern.ch/record/2767187 (cit. on p. 4).

[45] ATLAS Collaboration,
A precise measurement of the Z-boson double-differential transverse momentum and rapidity distributions in the full phase space of the decay leptons with the ATLAS experiment at $\sqrt{s} = 8$ TeV,
ATLAS-CONF-2023-013, 2023 (cit. on pp. 4, 5).

[46] J. C. Collins and D. E. Soper, *Angular Distribution of Dileptons in High-Energy Hadron Collisions*,
Phys. Rev. D **16** (1977) 2219 (cit. on p. 5).

[47] E. Mirkes, *Angular decay distribution of leptons from W-bosons at NLO in hadronic collisions*,
Nucl. Phys. B **387** (1992) 3 (cit. on p. 5).

[48] S. Camarda, L. Cieri and G. Ferrera,
Drell–Yan lepton-pair production: q_T resummation at approximate N^4LL+N^4LO accuracy, (2023),
arXiv: 2303.12781 [hep-ph] (cit. on p. 5).

[49] J. C. Collins, D. E. Soper and G. F. Sterman,
Transverse Momentum Distribution in Drell-Yan Pair and W and Z Boson Production,
Nucl. Phys. B **250** (1985) 199 (cit. on pp. 5, 12, 15).

[50] G. Bozzi, S. Catani, D. de Florian and M. Grazzini,
Transverse-momentum resummation and the spectrum of the Higgs boson at the LHC,
Nucl. Phys. B **737** (2006) 73, arXiv: hep-ph/0508068 (cit. on p. 5).

[51] S. Catani, D. de Florian, G. Ferrera and M. Grazzini, *Vector boson production at hadron colliders: transverse-momentum resummation and leptonic decay*, JHEP **12** (2015) 047,
arXiv: 1507.06937 [hep-ph] (cit. on p. 5).

[52] R. Boughezal et al.,
Z-boson production in association with a jet at next-to-next-to-leading order in perturbative QCD,
Phys. Rev. Lett. **116** (2016) 152001, arXiv: 1512.01291 [hep-ph] (cit. on p. 5).

[53] S. Camarda, L. Cieri and G. Ferrera,
Fiducial perturbative power corrections within the $\mathbf{q}_T$ subtraction formalism,
Eur. Phys. J. C **82** (2022) 575, arXiv: 2111.14509 [hep-ph] (cit. on p. 5).

[54] J. Collins and T. Rogers, *Understanding the large-distance behavior of transverse-momentum-dependent parton densities and the Collins-Soper evolution kernel*,
Phys. Rev. D **91** (2015) 074020, arXiv: 1412.3820 [hep-ph] (cit. on pp. 5, 12).

[55] J. McGowan, T. Cridge, L. A. Harland-Lang and R. S. Thorne, *Approximate N^3LO parton distribution functions with theoretical uncertainties: MSHT20aN^3LO PDFs*,
Eur. Phys. J. C **83** (2023) 185, arXiv: 2207.04739 [hep-ph] (cit. on pp. 5, 13, 14).

[56] A. Buckley et al., *LHAPDF6: parton density access in the LHC precision era*,
Eur. Phys. J. C **75** (2015) 132, arXiv: 1412.7420 [hep-ph] (cit. on p. 5).

[57] T. Sjöstrand et al., *An introduction to PYTHIA 8.2*, Comput. Phys. Commun. **191** (2015) 159,
arXiv: 1410.3012 [hep-ph] (cit. on p. 6).

[58] L. Cieri, G. Ferrera and G. F. R. Sborlini, *Combining QED and QCD transverse-momentum resummation for Z boson production at hadron colliders*, JHEP **08** (2018) 165,
arXiv: 1805.11948 [hep-ph] (cit. on pp. 6, 7).

[59] S. Bondarenko, Y. Dydyshka, L. Kalinovskaya, R. Sadykov and V. Yermolchyk,
Hadron-hadron collision mode in ReneSANCe-v1.3.0, Comput. Phys. Commun. **285** (2023) 108646,
arXiv: 2207.04332 [hep-ph] (cit. on p. 6).

[60] S. Alekhin et al., *HERAFitter*, Eur. Phys. J. C **75** (2015) 304, arXiv: 1410.4412 [hep-ph]
(cit. on p. 6).

[61] S. Camarda et al., *QCD analysis of W- and Z-boson production at Tevatron*,
Eur. Phys. J. C **75** (2015) 458, arXiv: 1503.05221 [hep-ph] (cit. on pp. 6, 13).

[62] F. Herren and M. Steinhauser, *Version 3 of RunDec and CRunDec*,
Comput. Phys. Commun. **224** (2018) 333, arXiv: 1703.03751 [hep-ph] (cit. on p. 7).

[63] H. Abramowicz et al., *Combination of measurements of inclusive deep inelastic $e^{\pm}p$ scattering cross sections and QCD analysis of HERA data*, Eur. Phys. J. C **75** (2015) 580,
arXiv: 1506.06042 [hep-ex] (cit. on pp. 9, 14).

[64] C. T. H. Davies, B. R. Webber and W. J. Stirling,
Drell-Yan cross sections at small transverse momentum, Nucl. Phys. B **256** (1985) 413 (cit. on p. 12).

[65] G. A. Ladinsky and C. P. Yuan,
Nonperturbative regime in QCD resummation for gauge boson production at hadron colliders, Phys. Rev. D **50** (1994) R4239, arXiv: hep-ph/9311341 (cit. on p. 12).

[66] R. K. Ellis, D. A. Ross and S. Veseli, *Vector boson production in hadronic collisions*, Nucl. Phys. B **503** (1997) 309, arXiv: hep-ph/9704239 (cit. on p. 12).

[67] F. Landry, R. Brock, G. Ladinsky and C. P. Yuan,
New fits for the non-perturbative parameters in the CSS resummation formalism, Phys. Rev. D **63** (2000) 013004, arXiv: hep-ph/9905391 (cit. on p. 12).

[68] J. Qiu and X. Zhang,
Role of the nonperturbative input in QCD resummed Drell-Yan Q_T distributions, Phys. Rev. D **63** (2001) 114011, arXiv: hep-ph/0012348 (cit. on p. 12).

[69] A. Kulesza, G. F. Sterman and W. Vogelsang, *Joint resummation in electroweak boson production*, Phys. Rev. D **66** (2002) 014011, arXiv: hep-ph/0202251 (cit. on p. 12).

[70] A. V. Konychev and P. M. Nadolsky,
Universality of the Collins-Soper-Sterman nonperturbative function in vector boson production, Phys. Lett. B **633** (2006) 710, arXiv: hep-ph/0506225 (cit. on p. 12).

[71] M. Guzzi, P. M. Nadolsky and B. Wang, *Nonperturbative contributions to a resummed leptonic angular distribution in inclusive neutral vector boson production*, Phys. Rev. D **90** (2014) 014030, arXiv: 1309.1393 [hep-ph] (cit. on p. 12).

[72] S. Wei, *Exploring the non-perturbative Sudakov factor via Z^0 -boson production in pp collisions*, Phys. Lett. B **817** (2021) 136356, arXiv: 2009.06514 [hep-ph] (cit. on p. 12).

[73] S. Tafat, *Nonperturbative corrections to the Drell-Yan transverse momentum distribution*, JHEP **05** (2001) 004, arXiv: hep-ph/0102237 (cit. on p. 12).

[74] S. Ferrario Ravasio, G. Limatola and P. Nason,
Infrared renormalons in kinematic distributions for hadron collider processes, JHEP **06** (2021) 018, arXiv: 2011.14114 [hep-ph] (cit. on p. 12).

[75] F. Caola, S. Ferrario Ravasio, G. Limatola, K. Melnikov and P. Nason,
On linear power corrections in certain collider observables, JHEP **01** (2022) 093, arXiv: 2108.08897 [hep-ph] (cit. on p. 12).

[76] J. C. Collins and D. E. Soper, *Back-to-back jets: Fourier transform from b to k_T*, Nucl. Phys. B **197** (1982) 446 (cit. on p. 12).

[77] P. Schweitzer, M. Strikman and C. Weiss,
Intrinsic transverse momentum and parton correlations from dynamical chiral symmetry breaking, JHEP **01** (2013) 163, arXiv: 1210.1267 [hep-ph] (cit. on p. 12).

[78] R. D. Ball et al., *The path to proton structure at 1% accuracy*, Eur. Phys. J. C **82** (2022) 428, arXiv: 2109.02653 [hep-ph] (cit. on p. 14).

[79] T.-J. Hou et al.,
New CTEQ global analysis of quantum chromodynamics with high-precision data from the LHC, Phys. Rev. D **103** (2021) 014013, arXiv: 1912.10053 [hep-ph] (cit. on p. 14).

[80] S. Forte and Z. Kassabov, *Why α_s cannot be determined from hadronic processes without simultaneously determining the parton distributions*, Eur. Phys. J. C **80** (2020) 182, arXiv: 2001.04986 [hep-ph] (cit. on p. 14).

[81] H. Paukkunen and P. Zurita, *PDF reweighting in the Hessian matrix approach*, JHEP **12** (2014) 100, arXiv: 1402.6623 [hep-ph] (cit. on p. 14).

[82] S. Agarwal, K. Mierle and T. C. S. Team, *Ceres Solver*, version 2.1, 2022, URL: https://github.com/ceres-solver/ceres-solver (cit. on p. 14).

[83] S. Weinberg, *New approach to the renormalization group*, Phys. Rev. D **8** (1973) 3497 (cit. on p. 14).

[84] R. S. Thorne and R. G. Roberts, *Ordered analysis of heavy flavor production in deep-inelastic scattering*, Phys. Rev. D **57** (1998) 6871, arXiv: hep-ph/9709442 (cit. on p. 14).

[85] R. S. Thorne, *Variable-flavor number scheme for next-to-next-to-leading order*, Phys. Rev. D **73** (2006) 054019, arXiv: hep-ph/0601245 (cit. on p. 14).

[86] R. S. Thorne, *Effect of changes of variable flavor number scheme on parton distribution functions and predicted cross sections*, Phys. Rev. D **86** (2012) 074017, arXiv: 1201.6180 [hep-ph] (cit. on p. 14).

[87] M. Bonvini and F. Giuli, *A new simple PDF parametrization: improved description of the HERA data*, Eur. Phys. J. Plus **134** (2019) 531, arXiv: 1902.11125 [hep-ph] (cit. on p. 15).

[88] G. Billis, F. J. Tackmann and J. Talbert, *Higher-Order Sudakov Resummation in Coupled Gauge Theories*, JHEP **03** (2020) 182, arXiv: 1907.02971 [hep-ph] (cit. on p. 15).

[89] V. Bertone, G. Bozzi and F. Hautmann, *Perturbative hysteresis and emergent resummation scales*, Phys. Rev. D **105** (2022) 096003, arXiv: 2202.03380 [hep-ph] (cit. on p. 15).